



Azine-based covalent organic frameworks as metal-free visible light photocatalysts for CO₂ reduction with H₂O

Yanghe Fu^a, Xiaoli Zhu^a, Liang Huang^b, Xincong Zhang^a, Fumin Zhang^a, Weidong Zhu^{a,*}

^a Key Laboratory of the Ministry of Education for Advanced Catalysis Materials, Institute of Physical Chemistry, Zhejiang Normal University, Jinhua 321004, China

^b The State Key Laboratory of Refractories and Metallurgy, Wuhan University of Science and Technology, Wuhan 430081, China



ARTICLE INFO

Keywords:

Photocatalysis
Covalent organic frameworks
CO₂ reduction
Methanol
Visible light

ABSTRACT

The conversion of CO₂ into valuable organic products by means of solar energy is one of the best solutions to both global warming and energy shortage. Covalent organic frameworks (COFs) show a superior thermal and chemical stability due to their covalent bonds, besides, azine-based COFs, an interesting new class of photoactive materials, can combine advantages in CO₂ capture and heterogeneous photocatalysis for the conversion of CO₂. Here, for the first time two azine-based COFs were used as photocatalysts that catalyzed the reaction of CO₂ with H₂O into methanol under visible-light irradiation without any sacrificial agents. In addition, these azine-based COFs were more active in the photocatalytic reduction of CO₂ with H₂O than g-C₃N₄ and other reported photocatalysts coupling with inorganic semiconductors. Various techniques were used to characterize the synthesized azine-based COFs in combination with molecular simulation to elucidate the differences in the photocatalytic reduction of CO₂ between the two azine-based COFs investigated. The current work indicates that azine-based COFs would be ideal metal-free organic semiconductors, which might be developed into new flexible photocatalysts for CO₂ reduction due to their tunable composition, structure, and property. Furthermore, the present study would stimulate research and development in COFs-based photocatalysts and other new photocatalysts as energy transducers.

1. Introduction

The current energy production is mainly based on the combustion of non-renewable fossil fuels, in which large amounts of CO₂ are formed. Thus energy shortage and global warming caused by the emitted CO₂ have become the focus of world attention. The conversion of CO₂ into valuable chemicals and/or fuels utilizing solar energy is one of the most promising approaches to solve these problems [1]. Ever since the discovery of the photoelectrocatalytic reduction of CO₂ to organic compounds in the presence of TiO₂ suspension, a wide interest in the study of the photocatalytic reduction of CO₂ over semiconductors as catalysts has emerged and many semiconductors, such as TiO₂, CdS, ZnGa₂O₄, and Zn₂GeO₄ et al., have been found to be photocatalytically active in CO₂ reduction [2–7]. Although over most of the semiconductor photocatalysts investigated H₂O can be used as a reductant, their photocatalytic efficiency for CO₂ reduction and their selectivity for desired products are still quite low due to their limited visible-light harvesting, low adsorption capacity and selectivity for CO₂ and/or rapid charge recombination. Then transition metals modified mesoporous materials, such as Ti-MCM-41, Ti-MCM-48, and ZrCu(I)-MCM-41, consist another

important type of photocatalysts for CO₂ reduction because of the existence of ligand-to-metal charge-transfer (LMCT) or metal-metal charge transfer (MMCT) [8–10]. Nevertheless, most of them are only active in the ultraviolet (UV) region and their poor tunability inherent in these mesoporous materials-based photocatalysts limits their application in photocatalysis. Although homogeneous systems show a relatively high efficiency for solar CO₂ fixation in the presence of strong organic sacrificial agents, unfortunately, most of the involved systems are limited to noble-metal catalysts that are usually unrecyclable [11–15].

Recently, some investigators have demonstrated the application of metal-organic frameworks (MOFs)-based photocatalysts in CO₂ reduction [16–22]. It has been reported that in MOFs the metal-oxo clusters could act as inorganic semiconducting quantum dots while the organic linkers serve as antennas to activate these semiconducting quantum dots by the LMCT upon photoexcitation, thus making MOFs-based photocatalysis possible [23,24]. In addition, MOFs are usually good at CO₂ capture due to their large surface area, high porosity, and tunable interactions with CO₂, facilitating the photocatalytic reduction of CO₂. However, in the current photocatalytic reduction of CO₂ over MOFs,

* Corresponding author.

E-mail address: weidongzhu@zjnu.cn (W. Zhu).

triethanolamine (TEOA) is often used as a sacrificial electron donor [25–31], which is not economical and environment-friendly enough, because: 1) TEOA cannot be converted to valuable products, just as a sacrificial hole scavenger; 2) the excessive emission of TEOA will cause the environmental pollution; and 3) the use of TEOA will lead to the laborious purification of the produced HCOOH due to the strong intermolecular interactions between the formed acid-base adducts. Thus it would be ideal if H_2O could be used as a reductant, coupling the photochemical reduction of CO_2 with the photochemical splitting of H_2O . Unfortunately, most of MOFs undergo an extensive decomposition in H_2O . Additionally, a practical application of MOFs would be hindered by their poor thermal and chemical stability, which originates from their weak metal-linker coordination bonds. Therefore, it would be of great significance to develop visible-light-responsive and highly efficient photocatalysts for CO_2 reduction with H_2O .

Covalent organic frameworks (COFs) represent an exciting new type of porous organic materials, which are ingeniously constructed with organic building units via strong covalent bonds. The well-defined crystalline porous structures together with tailored functionalities have offered the COF materials superior potential in diverse applications, such as gas storage, adsorption, catalysis, organic electronics, chemosensing and energy storage [32–35]. Some COFs with interesting optoelectronic properties and charge separation capabilities have emerged recently [36], suggesting that COFs could be ideal metal-free organic semiconductors to be developed for new flexible photocatalysts. As an organic semiconductor, graphitic carbon nitride ($g-C_3N_4$) has been widely investigated as photocatalyst and shows an effective performance in solar energy conversion and environmental remediation due to its appealing electronic band structure, high physicochemical stability, and “earth-abundant” nature [37–40]. Similar to $g-C_3N_4$, the π -stacked structure of COFs as organic semiconductors provides defined pathways for charge-carrier transport [41]. Besides, a distinct advantage of COFs is that their physicochemical properties, such as porosity and photochemical activity, can be systematically controlled by the right choice of the monomers used in their syntheses. Therefore, azine-based COFs with π -stacked aromatic units, as typical COFs, would be expected to promote exciton separation and charge transport, which are preferred to photocatalysis [36]. Recently, a small number of azine-based COFs as photocatalysts for H_2O splitting have been studied due to their high chemical and thermal stability [42–49]. For example, 2D azine-linked COFs from hydrazine and triphenylarene aldehydes with a varying number of nitrogen atoms (N_x –COF, in which x represents the number of nitrogen atoms) can be tuned for visible light-induced hydrogen evolution from H_2O . The average amount of hydrogen produced by N_3 –COF can be up to $1703 \mu\text{mol g}^{-1} \text{h}^{-1}$ under visible light irradiation [46]. Compared with traditional semiconductors and MOFs, azine-based COFs as photocatalysts for CO_2 reduction have the following advantages: 1) the COFs with diverse structures can be easily designed, modified, and modulated, which make them attractive in photocatalysis; 2) similar to MOFs, the COFs possess large surface areas and abundant nitrogen atoms in their skeleton, leading to a higher adsorption capacity and selectivity for CO_2 than those of traditional semiconductors; and 3) the COFs have a better thermal and chemical stability than MOFs due to their strong covalent bonds. Therefore, it can be anticipated that azine-based COFs could potentially combine advantages in CO_2 capture and heterogeneous photocatalysis to be used for the conversion of CO_2 with H_2O . To the best of our knowledge, the application of azine-based COFs as metal-free photocatalysts with visible-light response in CO_2 reduction has not been reported yet.

Herein, two azine-linked 2D COFs, named as ACOF-1 and N_3 –COF, respectively, are applied in the photocatalytic reduction of CO_2 with H_2O upon visible light irradiation. The exploration of azine-linked COFs with diverse and easily tailored structure in CO_2 reduction may not only widen the scope of organic semiconductors but also provide a molecular-level understanding of the inherent heterogeneous photocatalysis.

2. Experimental

2.1. Materials

All reagents with AR purity (analytical reagent grade) were used as received without further purification. Mesitylene, 1,4-dioxane, 1,3,5-triformylbenzene (TFB), 2,4,6-tris(4-bromophenyl)-1,3,5-triazine (N_3 -Br), melamine, acetic acid, hydrazine hydrate (50–60% solution), chloroform, tetrahydrofuran (THF), acetone, hydrochloric acid (HCl), anhydrous magnesium sulfate ($MgSO_4$), N-formylpiperidine, dichloromethane, and *n*-butyllithium (*n*-BuLi, 2.5 M in hexane) were purchased from Sigma Aldrich Co.

2.2. Synthesis

The synthesis of ACOF-1 and N_3 –COF was adapted from the recipe from the literature with some modification [35,46].

ACOF-1. TFB (60 mg, 0.37 mmol), hydrazine hydrate (38 μL , 0.56 mmol), dioxane (2 mL), and acetic acid (0.2 mL, 6 M) were mixed in a 10 mL glass vial. The obtained mixture was sonicated for 2 min and then sealed under argon. The reaction was kept in an oil bath at 120 °C for 72 h to get a light yellow solid at the bottom of the tube. The obtained solid was separated, washed with dioxane, THF, and acetone, and finally dried under vacuum at 100 °C for 10 h.

2,4,6-Tris(4-formylphenyl)-1,3,5-triazine (N_3 -Ald). 0.5 g of N_3 -Br (0.9 mmol) was dispersed with THF (150 mL) in a schlenk flask under argon flow at –78 °C. 1.1 mL of *n*-BuLi (2.7 mmol) was added to the suspension and stirred for 1 h. Then 0.32 mL of N-formylpiperidine (2.9 mmol) was added into the mixture, stirred for 30 min and then warmed up to room temperature. After stirred for another 1 h, 5 mL of HCl (0.5 M) was added. The mixture was extracted with dichloromethane, dried over anhydrous $MgSO_4$, and then filtered. Finally, the solvent was evaporated to get a white solid (0.25 g).

N_3 –COF. 40 μL of hydrazine hydrate was added into the suspension of N_3 -Ald (100 mg, 0.26 mmol) in a mixture of mesitylene (2.0 mL), 1,4-dioxane (2.0 mL), and aqueous acetic acid (200 μL , 6 M) in a 10 mL glass vial under argon flow. The glass vial was then sealed and heated in an oil bath at 120 °C for 72 h. Thereafter, the suspension was filtered, washed with chloroform (5 mL × 2), acetone (5 mL × 2), and THF (5 mL × 2), and finally dried under vacuum at 100 °C for 10 h to get N_3 –COF as light yellow powder.

$g-C_3N_4$. For comparison, $g-C_3N_4$ was prepared by annealing melamine in a muffle furnace [50]. Specifically, 10 g of melamine powder was placed in an alumina crucible and then heated to 550 °C for 4 h. After cooling to room temperature, the light yellow solid was ground to a fine powder.

2.3. Characterization

The X-ray powder diffraction (XRD) patterns were collected on a Rigaku Smart Lab automated powder diffraction system in a scanning range of 2–40 ° at 1°/min. The Fourier transform infrared (FT-IR) spectra of the samples were recorded on a Nicolet iS50 FT-IR spectrometer with a resolution of 4 cm^{-1} . The Brunauer-Emmett-Teller (BET) surface area was determined by N_2 adsorption/desorption at –196 °C using a Quantachrome Autosorb IQ automated gas adsorption analyzer. The sample was degassed in vacuum at 180 °C for 5 h prior to the adsorption measurement. The UV-vis diffuse reflectance spectra (UV-vis DRS) of the samples were recorded on a Cary 4000 UV-vis spectrophotometer (Varian) using MgO as reference from 250 nm to 800 nm.

2.4. Electrochemistry measurements

The electrochemical analysis was carried out in a conventional three electrode cell, using two Pt plates as counter and reference electrodes, respectively. The working electrode was prepared on fluorine-doped tin

oxide (FTO) glass, which was cleaned by sonication in deionized H₂O and ethanol for 30 min, and then dried. The FTO slide was dip-coated with 10 mL of slurry, which was obtained from the mixture of photocatalyst (5 mg) and H₂O (0.5 mL) under sonication for 2 h, and the side part of the FTO slide was previously protected using Scotch tape. After natural air-drying, a copper wire was connected to the side part of the FTO glass using a conductive tape. The uncoated parts of the electrode were isolated with an epoxy resin, and the exposed area of the electrode was 0.25 cm². The working electrodes were immersed in a 0.2 M Na₂SO₄ aqueous solution without any additive for 30 s prior to the measurement. The photocurrent measurements were conducted with a CHI440 A workstation (Shanghai Chenhua Instruments Co.). A 300 W Xe lamp (Beijing Perfectlight, PLS-SXE 300c) with a 420 nm cut-off filter was used as a light source.

2.5. Photocatalytic reaction

The schematic diagram of a set-up for the photocatalytic reduction of CO₂ is shown in Fig. S1 in the Supporting Information. A 500 W Xe lamp with a UV and an IR cutoff filter (800 nm $\geq \lambda \geq 420$ nm) was used as a light source, and the volume of the stainless steel reactor with a quartz window was 132 mL. 10 mg of photocatalyst was placed on a Teflon catalyst holder in the upper region of the reactor, and 5 mL of deionized H₂O was pre-injected into the bottom of the reactor. Prior to the light irradiation, the reactor was thoroughly purged by CO₂ to remove air from the inside of the reactor. The pressure of CO₂ and the temperature of the reactor were kept at 0.4 MPa and 80 °C, respectively, during the reaction. After light irradiation, the gas products were analyzed with an SRI 8610C gas chromatograph equipped with two FID detectors and one TCD detector, using 6' MS-13X, 6' HAYESEP-D, and 60 M MXT-1 columns, respectively. In addition, the produced CH₃OH from the photocatalytic reduction of ¹³CO₂ was also identified with an Agilent 7890A/5975C gas chromatography-mass spectrometer (GC-MS). To investigate the effects of CO₂ concentration on the photocatalytic reduction, pure CO₂ was diluted with N₂ to different volume concentrations. For the isotopic reaction, ¹³CO₂ was used instead of CO₂.

2.6. Simulation of ACOF-1 and N₃-COF crystalline structures

All simulations were performed using spin-polarization DFT/GGA with the PW91 exchange-correlation functional as implemented in the DMol3 package. A double numerical basis set augmented with polarization functions was used to describe the valence electrons, and all electron treatment was used to perform full optimization of ACOF-1 and N₃-COF. The convergence criteria were set to fine quality with a tolerance for self-consistent field (SCF), optimization energy, maximum force, and maximum displacement of 10⁻⁶ Ha, 1 × 10⁻⁵ Ha, 0.004 Ha/Å, and 0.005 Å, respectively. The simulation of the X-ray diffraction patterns of the two COFs was carried out using the Reflect Tools in Materials Studio.

3. Results and discussion

ACOF-1 and N₃-COF were synthesized using 1,3,5-triformylbenzene (TFB) and 2,4,6-tris(4-bromophenyl)-1,3,5-triazine (N₃-Ald), respectively, as the aldehyde component to condense with hydrazine hydrate. The calculated lattice parameters were $a = b = 14.724$ Å, $c = 3.310$ Å for ACOF-1 and $a = b = 28.979$ Å, $c = 3.447$ Å for N₃-COF, in good agreement with those reported in the literature [35,46]. In addition, the simulation of the crystalline structures indicates that both ACOF-1 and N₃-COF consist of AA stacking structure, whereas the phenyl groups at the vertices and the azine linkers on the edges of two-dimensional (2D) hexagon sheets stack to form periodic phenyl columns and one-dimensional channels with open azine units on the pore walls (Figs. S2 and 3 in the Supporting

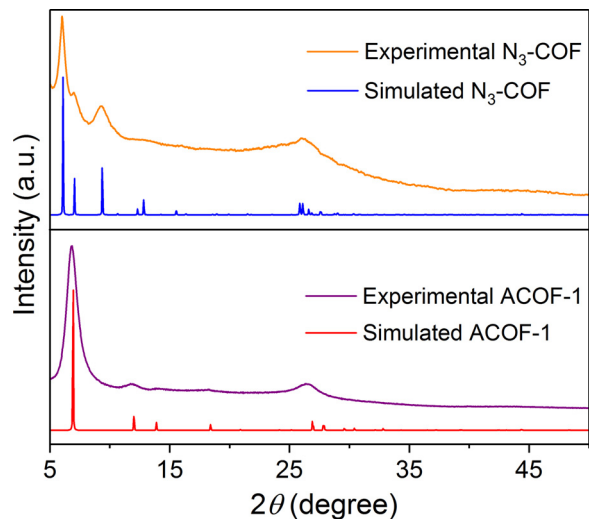


Fig. 1. Simulated and experimental XRD patterns of ACOF-1 and N₃-COF.

Information). The crystalline structures of ACOF-1 and N₃-COF were determined by the XRD measurement. The experimental XRD patterns of ACOF-1 and N₃-COF are consistent with the simulated ones, see Fig. 1. The reflections at 7.0, 12.0, 13.8, and 18.4° correspond to the (100), (110), (200), and (120) facets for ACOF-1 while the reflections at 6.0, 7.1, and 9.5° correspond to the (110), (200), and (120) facets for N₃-COF, respectively. A slightly broad peak at higher 2θ (~26°) is mainly due to π-π stacking between COF layers and corresponds to the (001) plane. The FT-IR spectra of ACOF-1 and N₃-COF indicate a typical stretching band arising from C=N at around 1621 cm⁻¹ (Fig. 2). A carbonyl stretching band around 1700 cm⁻¹ for the starting monomers N₃-Ald and TFB can be found in their FT-IR spectra while the carbonyl stretching band cannot be seen for N₃-COF and ACOF-1, demonstrating that the COFs possess a fully azine-linked network. The BET surface area of N₃-COF is 1412 m² g⁻¹, which is higher than that of ACOF-1 (1053 m² g⁻¹), as shown in Fig. 3. The high surface area and the abundant nitrogen sites on the surface are anticipated to a higher CO₂ adsorption capacity, facilitating the photocatalytic reduction of CO₂. The UV-vis diffuse reflectance spectra reveal that ACOF-1 and N₃-COF absorb light in the ultraviolet and blue parts of the visible region with an absorption edge at ~480–500 nm (Fig. 4), thereby suggesting an optical band gap of ~2.6 eV as determined by the Kubelka-Munk equation. To investigate the photoelectrochemical property of ACOF-1 and N₃-COF, the photocurrent measurement was carried

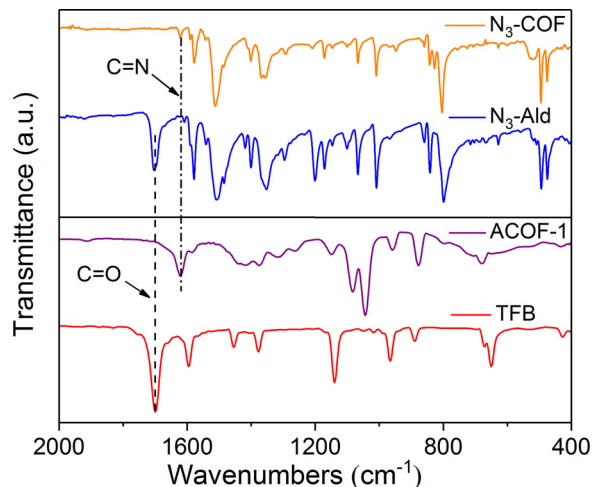


Fig. 2. FT-IR spectra of ACOF-1 and N₃-COF.

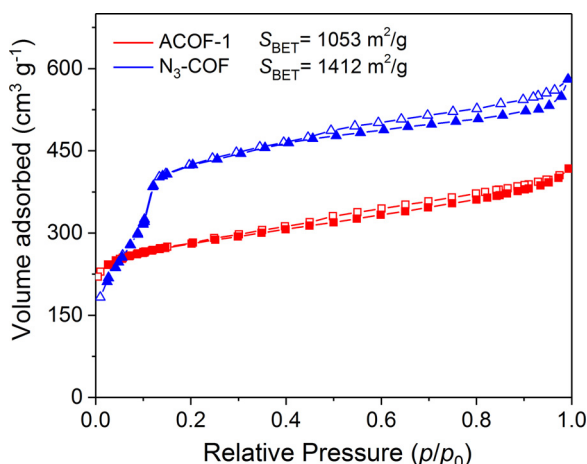


Fig. 3. Adsorption-desorption isotherms of N_2 on ACOF-1 and $\text{N}_3\text{-COF}$ at -196°C .

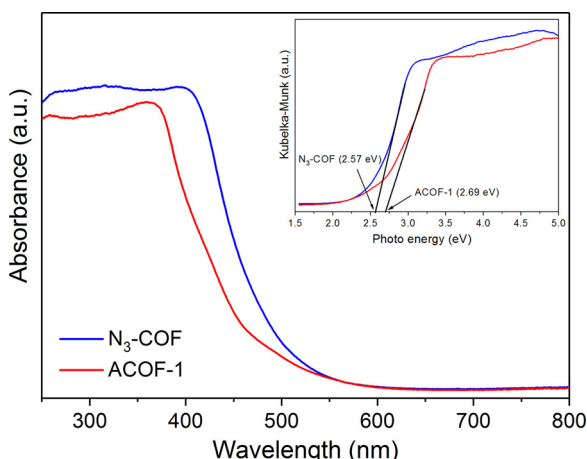


Fig. 4. UV-vis spectra of ACOF-1 and $\text{N}_3\text{-COF}$. The inset is the plot used to estimate the band gap value by the Kubelka-Munk equation.

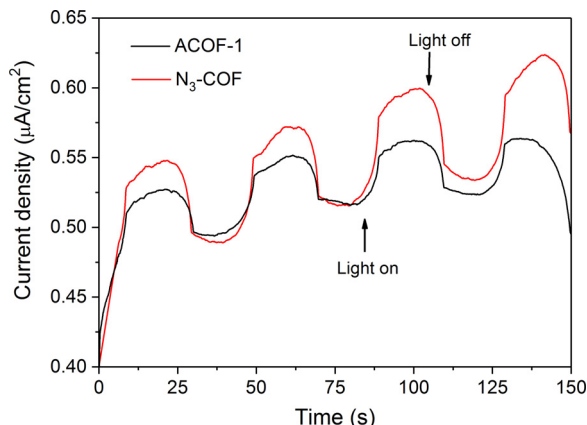


Fig. 5. Transient photocurrent responses of ACOF-1 (black) and $\text{N}_3\text{-COF}$ (red) in 0.2 M Na_2SO_4 aqueous solution without bias versus Ag/AgCl upon visible light irradiation ($\lambda \geq 420 \text{ nm}$) (For interpretation of the references to colour in this figure legend, the reader is referred to the web version of this article).

out under visible light irradiation ($\lambda \geq 420 \text{ nm}$). As shown in Fig. 5, the photocurrent generated by both samples with a reproducible response indicates that the photoinduced carriers transfer on the photoelectrode. In comparison with ACOF-1, $\text{N}_3\text{-COF}$ shows the enhancement of the long-term steady photocurrent density response, indicating that

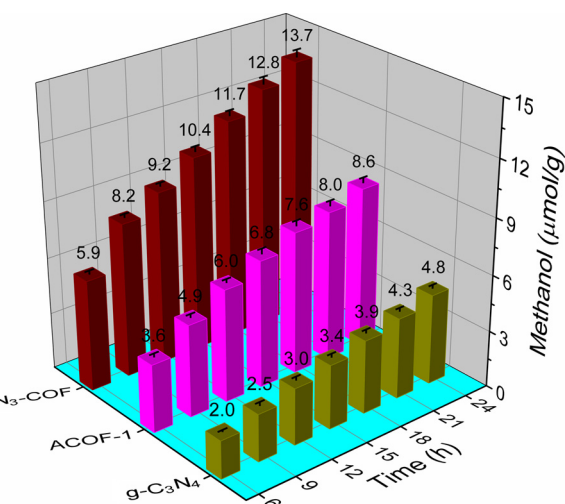


Fig. 6. Amount of the CH_3OH produced as a function of irradiation time using $\text{g-C}_3\text{N}_4$, ACOF-1 or $\text{N}_3\text{-COF}$ as photocatalyst. Reaction conditions: photocatalyst: 10 mg, H_2O : 5 mL, pressure: 0.4 MPa, temperature: 80°C .

$\text{N}_3\text{-COF}$ should possess a better photocatalytic activity for CO_2 reduction.

The photocatalytic reduction of CO_2 with H_2O was performed in a stainless steel reactor with a quartz window on the top of the reactor under visible light irradiation. The reaction was photocatalytic, because no product was detected without neither photocatalyst nor light irradiation. The main product over either ACOF-1 or $\text{N}_3\text{-COF}$ was CH_3OH in the gas phase, with a trace amount of H_2 and O_2 that could not be quantified due to their extremely low concentrations. The inactivity of the organic monomer TFB or $\text{N}_3\text{-Ald}$ under otherwise similar conditions confirms that the visible light photocatalytic activity for CO_2 reduction is actually induced by either ACOF-1 or $\text{N}_3\text{-COF}$. A temporal concentration change of CH_3OH as a function of irradiation time shows that the amount of CH_3OH formed over $\text{N}_3\text{-COF}$ is $13.7 \mu\text{mol/g}$ in 24 h, much higher than that over ACOF-1 (Fig. 6). Under similar reaction conditions, the current COFs for CO_2 reduction are more active than $\text{g-C}_3\text{N}_4$ and those coupled with semiconductors reported by others [51–53]. This could be ascribed to a higher adsorption affinity of the azine-based COFs to CO_2 , compared to that of $\text{g-C}_3\text{N}_4$. In addition, the influence of CO_2 concentration on the photocatalytic reduction of CO_2 was investigated as well, see Fig. 7. A decrease in CO_2 concentration suppresses the photoreduction of CO_2 . Nevertheless, when CO_2 concentration is as low as 1% (diluted by nitrogen), the yield of CH_3OH over $\text{N}_3\text{-COF}$ is still as high as $9.9 \mu\text{mol/g}$, probably due to the high selective adsorption of CO_2 on the catalyst. On the other hand, in comparison, the yield of CH_3OH over $\text{g-C}_3\text{N}_4$ is much lower. Thus these azine-based COFs are more competitive than $\text{g-C}_3\text{N}_4$ in the photocatalytic reduction of CO_2 .

To study the origin of CH_3OH , the isotopic $^{13}\text{CO}_2$ was used for the photocatalytic reaction and the obtained product was identified by the GC-MS (Fig. S4 in the Supporting Information). Most of the m/z values in the mass spectra of the produced methanol from the reaction with $^{13}\text{CO}_2$ are larger than those of the reaction with CO_2 by 1 unit, confirming that the produced CH_3OH originates from CO_2 . Finally, the stability of $\text{N}_3\text{-COF}$ as an illustrative example was investigated by a five-run cycling test of photocatalytic CO_2 reduction (Fig. S5 in the Supporting Information). The result reveals that the yield of CH_3OH only slightly decreases in the first two cycling runs, verifying the reusability of $\text{N}_3\text{-COF}$. Additionally, the XRD, FT-IR, and N_2 adsorption-desorption characterization results of $\text{N}_3\text{-COF}$ after the 5th-run reaction are almost identical to those for the fresh one (Figs. S6–8 in the Supporting Information), further confirming the stability of $\text{N}_3\text{-COF}$ during the photocatalytic reduction of CO_2 .

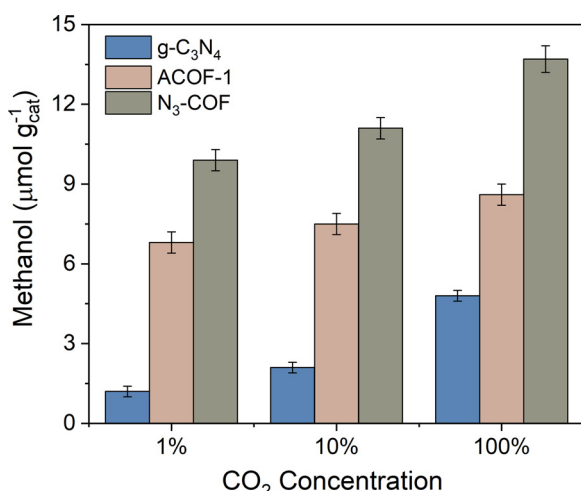


Fig. 7. Effects of CO₂ concentration on the photocatalytic performance of g-C₃N₄, ACOF-1 or N₃-COF under visible light irradiation. Reaction conditions: photocatalyst: 10 mg, H₂O: 5 mL, pressure: 0.4 MPa, temperature: 80 °C, irradiation time: 24 h.

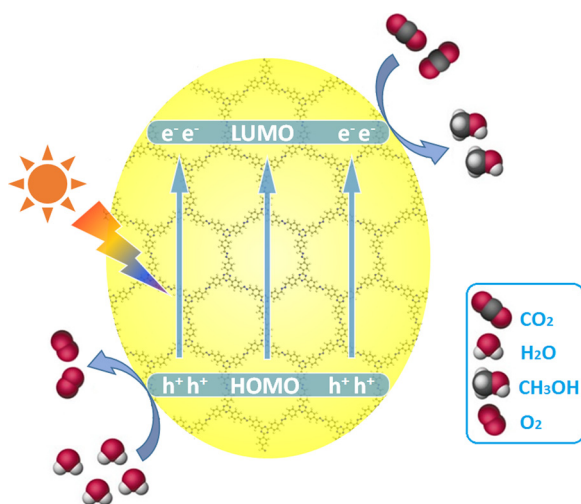


Fig. 8. Schematic diagram for the photocatalytic reduction of CO₂ over azine-based COFs upon visible light irradiation.

It's well known that the highest occupied molecular orbital (HOMO) and the lowest unoccupied molecular orbital (LUMO) are often invoked to rationalize exciton delocalization, charge separation, and location of potential charge-transfer sites. Hence, the density functional theory (DFT) calculations were performed to study the electronic and conformational details based on the optimized structures of ACOF-1 and N₃-COF. It should be mentioned that triazine and phenyl groups in both ACOF-1 and N₃-COF are coplanar (Figs. S9–12 in the Supporting Information), suggesting a strong conjugation effect. Taking N₃-COF as an example, the HOMO is localized solely on the triazine linker unit while the LUMO is delocalized across the conjugated π-system of the framework. The electronic distributions of N₃-COF at the HOMO and the LUMO have a good electron-separated state and well-over lapped orbital, which is conducive to the intramolecular charge transfer transition. By calculating, the HOMO and LUMO energy levels can be predicted as -5.00 and -2.54 eV for ACOF-1, -4.95 and -2.71 eV for N₃-COF, respectively. In principle, the observed HOMO-LUMO gap of either ACOF-1 or N₃-COF is large enough to enable CO₂ reduction through band gap excitation and at the same time small enough to harvest a significant portion of the visible light spectrum. When associating the HOMO with the charge-transfer sites for holes, it could be

inferred that efficient hole quenching is possible through hydrogen-bonding interactions with H₂O via the azine moiety while the excited electrons from the LUMO energy level can react with the adsorbed CO₂ on the catalyst surface to produce methanol, as shown in Fig. 8. Compared with ACOF-1, N₃-COF with electron-poor character of triazine building blocks shows more efficient at stabilizing the negative charge generated on the COF, which is important for the photocatalytic process to get a better activity [46]. This is consistent with the results from photocurrent experiments and photocatalytic reactions.

4. Conclusions

The photocatalytic reduction of CO₂ with H₂O into CH₃OH under visible light irradiation without any sacrificial agents is for the first time realized over the two metal-free azine-based COFs, ACOF-1 and N₃-COF. This work highlights the potential of COFs as photocatalysts for the reduction of CO₂. Although the activity for the reduction of CO₂ over the current catalysts is still low, considering the availability of different organic linkers, and the possibility to modulate the composition, structure, and properties of COFs, high-efficient COFs-based photocatalysts for the reduction of CO₂ could be obtained. In addition, the present study would stimulate research and development in COFs-based photocatalysts and other new photocatalysts for CO₂ reduction.

Acknowledgements

This work is financially supported by Zhejiang Provincial Natural Science Foundation of China (LY18B030006), National Natural Science Foundation of China (21476214, 21576243 and 21303166), and the Programme of Introducing Talents of Discipline to Universities (D17008).

Appendix A. Supplementary data

Supplementary material related to this article can be found, in the online version, at doi:<https://doi.org/10.1016/j.apcatb.2018.08.004>.

References

- [1] Y. Zheng, W. Zhang, Y. Li, J. Chen, B. Yu, J. Wang, L. Zhang, J. Zhang, Energy related CO₂ conversion and utilization: advanced materials/nanomaterials, reaction mechanisms and technologies, *Nano Energy* 40 (2017) 512–539.
- [2] M.E. El-Khouly, E. El-Mohsawy, S. Fukuzumi, Solar energy conversion: from natural to artificial photosynthesis, *J. Photochem. Photobiol. C: Photochem. Rev.* 31 (2017) 36–83.
- [3] T. Inoue, A. Fujishima, S. Konishi, K. Honda, Photoelectrocatalytic reduction of carbon dioxide in aqueous suspensions of semiconductor powders, *Nature* 277 (1979) 637–638.
- [4] K. Ravindranathan Thampi, J. Kiwi, M. Grätzel, Methanation and photo-methanation of carbon dioxide at room temperature and atmospheric pressure, *Nature* 327 (1987) 506–508.
- [5] W. Tu, Y. Zhou, Z. Zou, Photocatalytic conversion of CO₂ into renewable hydrocarbon fuels: state-of-the-art accomplishment, challenges, and prospects, *Adv. Mater.* 26 (2014) 4607–4626.
- [6] S.N. Haberreutinger, L. Schmidt-Mende, J.K. Stolarczyk, Photocatalytic reduction of CO₂ on TiO₂ and other semiconductors, *Angew. Chem. Int. Ed.* 52 (2013) 7372–7408.
- [7] G. Zhao, X. Huang, X. Wang, X. Wang, Progress in catalyst exploration for heterogeneous CO₂ reduction and utilization: a critical review, *J. Mater. Chem. A* 5 (2017) 21625–21649.
- [8] M. Anpo, Photocatalytic reduction of CO₂ with H₂O on highly dispersed Ti-oxide catalysts as a model of artificial photosynthesis, *J. CO₂ Util.* 1 (2013) 8–17.
- [9] W. Lin, H. Frei, Photochemical CO₂ splitting by metal-to-metal charge-transfer excitation in mesoporous ZrCu(I)-MCM-41 silicate sieve, *J. Am. Chem. Soc.* 127 (2005) 1610–1611.
- [10] J. Schneider, M. Matsuoka, M. Takeuchi, J. Zhang, Y. Horiuchi, M. Anpo, D.W. Bahnemann, Understanding TiO₂ photocatalysis: mechanisms and materials, *Chem. Rev.* 114 (2014) 9919–9986.
- [11] Y. Kuninobu, K. Takai, Organic reactions catalyzed by rhenium carbonyl complexes, *Chem. Rev.* 111 (2011) 1938–1953.
- [12] V. Artero, M. Fontecave, Solar fuels generation and molecular systems: Is it homogeneous or heterogeneous catalysis? *Chem. Soc. Rev.* 42 (2013) 2338–2356.
- [13] Y. Yamazaki, H. Takeda, O. Ishitani, Photocatalytic reduction of CO₂ using metal complexes, *J. Photochem. Photobiol. C: Photochem. Rev.* 25 (2015) 106–137.

- [14] S. Sato, T. Morikawa, T. Kajino, O. Ishitani, A highly efficient mononuclear iridium complex photocatalyst for CO₂ reduction under visible light, *Angew. Chem. Int. Ed.* 52 (2013) 988–992.
- [15] H. Takeda, C. Cometto, O. Ishitani, M. Robert, Electrons, photons, protons and earth-abundant metal complexes for molecular catalysis of CO₂ reduction, *ACS Catal.* 7 (2016) 70–88.
- [16] Y. Chen, D. Wang, X. Deng, Z. Li, Metal-organic frameworks (MOFs) for photocatalytic CO₂ reduction, *Catal. Sci. Technol.* 7 (2017) 4893–4904.
- [17] A. Dhakshinamoorthy, A.M. Asiri, H. García, Metal-organic framework (MOF) compounds: photocatalysts for redox reactions and solarfuel production, *Angew. Chem. Int. Ed.* 55 (2016) 5414–5445.
- [18] T. Zhang, W. Lin, Metal-organic frameworks for artificial photosynthesis and photocatalysis, *Chem. Soc. Rev.* 43 (2014) 5982–5993.
- [19] S. Wang, X. Wang, Imidazolium ionic liquids, imidazolylidene heterocyclic carbenes, and zeolitic imidazolate frameworks for CO₂ capture and photochemical reduction, *Angew. Chem. Int. Ed.* 55 (2016) 2308–2320.
- [20] J.W. Maina, C. Pozo-Gonzalo, L. Kong, J. Schütz, M. Hill, L.F. Dumée, Metal organic framework based catalysts for CO₂ conversion, *Mater. Horiz.* 4 (2017) 345–361.
- [21] C.A. Trickett, A. Helal, B.A. Al-Maythalony, Z.H. Yamani, K.E. Cordova, O.M. Yaghi, The chemistry of metal-organic frameworks for CO₂ capture, regeneration and conversion, *Nat. Rev. Mater.* 2 (2017) 17045.
- [22] H. He, J.A. Perman, G. Zhu, S. Ma, Metal-organic frameworks for CO₂ chemical transformations, *Small* 12 (2016) 6309–6324.
- [23] F.X. Llabrés i Xamena, A. Corma, H. García, Applications for metal-organic frameworks (MOFs) as quantum dot semiconductors, *J. Phys. Chem. C* 111 (2007) 80–85.
- [24] D. Sun, Y. Fu, W. Liu, L. Ye, D. Wang, L. Yang, X. Fu, Z. Li, Studies on photocatalytic CO₂ reduction over NH₂-UiO-66(Zr) and its derivatives: towards a better understanding of photocatalysis on metal-organic frameworks, *Chem. Eur. J.* 19 (2013) 14279–14285.
- [25] Y. Fu, D. Sun, Y. Chen, R. Huang, Z. Ding, X. Fu, Z. Li, An amine-functionalized titanium metal-organic framework photocatalyst with visible-light-induced activity for CO₂ reduction, *Angew. Chem. Int. Ed.* 51 (2012) 3364–3367.
- [26] H.-Q. Xu, J. Hu, D. Wang, Z. Li, Q. Zhang, Y. Luo, S.-H. Yu, H.-L. Jiang, Visible-light photoreduction of CO₂ in a metal-organic framework: boosting electron-hole separation via electron trap states, *J. Am. Chem. Soc.* 137 (2015) 13440–13443.
- [27] D. Wang, R. Huang, W. Liu, D. Sun, Z. Li, Fe-based MOFs for photocatalytic CO₂ reduction: role of coordination unsaturated sites and dual excitation pathways, *ACS Catal.* 4 (2014) 4254–4260.
- [28] Y. Lee, S. Kim, J.K. Kang, S.M. Cohen, Photocatalytic CO₂ reduction by a mixed metal (Zr/Ti), mixed ligand metal-organic framework under visible light irradiation, *Chem. Commun.* 51 (2015) 5735–5738.
- [29] S. Zhang, L. Li, S. Zhao, Z. Sun, J. Luo, Construction of interpenetrated ruthenium metal-organic frameworks as stable photocatalysts for CO₂ reduction, *Inorg. Chem.* 54 (2015) 8375–8379.
- [30] C. Wang, Z. Xie, K.E. deKrafft, W. Lin, Doping metal-organic frameworks for water oxidation, carbon dioxide reduction, and organic photocatalysis, *J. Am. Chem. Soc.* 133 (2011) 13445–13454.
- [31] L. Shi, T. Wang, H. Zhang, K. Chang, J. Ye, Electrostatic self-assembly of nanosized carbon nitride nanosheet onto a zirconium metal-organic framework for enhanced photocatalytic CO₂ reduction, *Adv. Funct. Mater.* 25 (2015) 5360–5367.
- [32] C.S. Diercks, O.M. Yaghi, The atom, the molecule, and the covalent organic framework, *Science* 355 (2017) eaal1585.
- [33] N. Huang, P. Wang, D. Jiang, Covalent organic frameworks: a materials platform for structural and functional designs, *Nat. Rev. Mater.* 1 (2016) 16068.
- [34] A.P. Cote, Porous, crystalline, covalent organic frameworks, *Science* 310 (2005) 1166–1170.
- [35] Z. Li, X. Feng, Y. Zou, Y. Zhang, H. Xia, X. Liu, Y. Mu, A 2D azine-linked covalent organic framework for gas storage applications, *Chem. Commun.* 50 (2014) 13825–13828.
- [36] V.S. Vydas, V.W. Lau, B.V. Lotsch, Soft photocatalysis: organic polymers for solar fuel production, *Chem. Mater.* 28 (2016) 5191–5204.
- [37] Y. Zheng, L. Lin, B. Wang, X. Wang, Graphitic carbon nitride polymers toward sustainable photoredox catalysis, *Angew. Chem. Int. Ed.* 54 (2015) 12868–12884.
- [38] W.-J. Ong, L.-L. Tan, Y.H. Ng, S.-T. Yong, S.-P. Chai, Graphitic carbon nitride (g-C₃N₄)-based photocatalysts for artificial photosynthesis and environmental remediation: are we a step closer to achieving sustainability? *Chem. Rev.* 116 (2016) 7159–7329.
- [39] K.S. Lakhi, D.-H. Park, K. Al-Bahily, W. Cha, B. Viswanathan, J.-H. Choyd, A. Vinu, Mesoporous carbon nitrides: synthesis, functionalization, and applications, *Chem. Soc. Rev.* 46 (2017) 72–101.
- [40] S. Cao, J. Low, J. Yu, M. Jaroniec, Polymeric photocatalysts based on graphitic carbon nitride, *Adv. Mater.* 27 (2015) 2150–2176.
- [41] D.D. Medina, T. Sick, T. Bein, Photoactive and conducting covalent organic frameworks, *Adv. Energy Mater.* 7 (2017) 1700387.
- [42] L. Li, W. Lo, Z. Cai, N. Zhang, L. Yu, Donor-acceptor porous conjugated polymers for photocatalytic hydrogen production: the importance of acceptor comonomer, *Macromolecules* 49 (2016) 6903–6909.
- [43] S. Kuecken, A. Acharya, L. Zhi, M. Schwarze, R. Schomäcker, A. Thomas, Fast tuning of covalent triazine frameworks for photocatalytic hydrogen evolution, *Chem. Commun. (Camb.)* 53 (2017) 5854–5857.
- [44] J. Bi, W. Fang, L. Li, J. Wang, S. Liang, Y. He, M. Liu, L. Wu, Covalent triazine-based frameworks as visible light photocatalysts for the splitting of water, *Macromol. Rapid Commun.* 36 (2015) 1799–1805.
- [45] L. Stegbauer, K. Schwinghammer, B.V. Lotsch, A hydrazone-based covalent organic framework for photocatalytic hydrogen production, *Chem. Sci.* 5 (2014) 2789–2793.
- [46] V.S. Vydas, F. Haase, L. Stegbauer, G. Savasci, F. Podjaski, C. Ochsnerfeld, B.V. Lotsch, A tunable azine covalent organic framework platform for visible light-induced hydrogen generation, *Nat. Commun.* 6 (2015) 8508.
- [47] K. Schwinghammer, S. Hug, M.B. Mesch, J. Senkerd, B.V. Lotsch, Phenyl-triazine oligomers for light-driven hydrogen evolution, *Energy Environ. Sci.* 8 (2015) 3345–3353.
- [48] K. Wang, L.-M. Yang, X. Wang, L. Guo, G. Cheng, C. Zhang, S. Jin, B. Tan, A. Cooper, Covalent triazine frameworks via a low-temperature polycondensation approach, *Angew. Chem. Int. Ed.* 56 (2017) 14149–14153.
- [49] L. Li, W. Fang, P. Zhang, J. Bi, Y. He, J. Wang, W. Su, Sulfur-doped covalent triazine-based frameworks for enhanced photocatalytic hydrogen evolution from water under visible light, *J. Mater. Chem. A* 4 (2016) 12402–12406.
- [50] J. Fu, B. Zhu, C. Jiang, B. Cheng, W. You, J. Yu, Hierarchical porous O-doped g-C₃N₄ with enhanced photocatalytic CO₂ reduction activity, *Small* 13 (2017) 1603938.
- [51] T. Ohno, N. Murakami, T. Koyanagi, Y. Yang, Photocatalytic reduction of CO₂ over a hybrid photocatalyst composed of WO₃ and graphitic carbon nitride (g-C₃N₄) under visible light, *J. CO₂ Util.* 6 (2014) 17–25.
- [52] W. Yu, D. Xu, T. Peng, Enhanced photocatalytic activity of g-C₃N₄ for selective CO₂ reduction to CH₃OH via facile coupling of ZnO: a direct Z-scheme mechanism, *J. Mater. Chem. A* 3 (2015) 19936–19947.
- [53] T. Di, B. Zhu, B. Cheng, J. Yu, J. Xu, A direct Z-scheme g-C₃N₄/SnS₂ photocatalyst with superior visible-light CO₂ reduction performance, *J. Catal.* 352 (2017) 532–541.